CRYSTAL GROWTH & DESIGN

Article

Cite This: Cryst. Growth Des. 2019, 19, 2912−2918

pubs.acs.org/crystal

Morphology Control by Pulsed Laser in Chemical Deposition Illustrated in ZnO Crystal Growth

Siyu Liu[†] and C. Richard Liu*[,†,‡]

[†]School of Industrial Engineering (Materials and Manufacturing Group), Purdue University, West Lafayette, Indiana 47907, United States

[‡]Birck Nanotechnology Center, Purdue University, West Lafayette, Indiana 47907, United States

Supporting Information

ABSTRACT: The control of pulsed-laser-induced deposition was studied with the case of ZnO crystallization in a hydrothermal reaction. Crystal orientation, morphologies, and growth rate were observed to vary under different pulsed-laser irradiation conditions. Different energy barriers during nucleation and crystal growth processes were determined by stepped changes of input energy levels of a pulsed laser with the corresponding observations of the states of the material. Therefore, by precisely adjusting the pulsed-laser energy that overcomes a particular energy barrier, ZnO crystals with desired orientation and morphology could be obtained on a seedless substrate in a catalyst-free environment. Crystals varied in morphologies showed different behavior in laser-induced growth, and growth rates were orders of magnitude higher than those of other hydrothermal reactions. By analyzing crystal growth characteristics in the reaction/diffusion-limited region, a set of guidelines were defined to tune the dimensions of ZnO crystals. Laser-induced crystal growth will benefit nanomanufacturing by providing a practical tool to tune the morphology of nanomaterials in a precise and effective manner, and it will bring deeper insight into the thermodynamic and kinetic mechanisms in hydrothermal reactions.

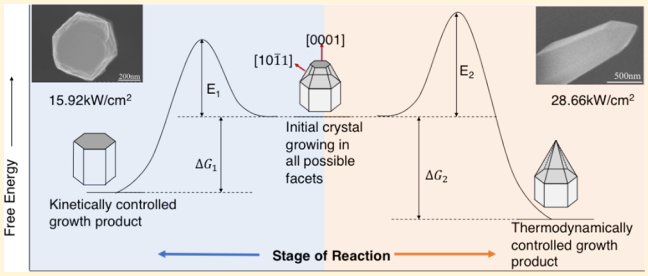

1. INTRODUCTION

Laser-induced chemical deposition could synthesize materials in selected positions. Previous studies showed that it was feasible for a great variety of nanomaterials to be produced efficiently through solution-based reactions. SnO_2, Fe_3O_4, MnO_2, ZnS, etc., were successfully deposited by a pulsed-laser method in previous studies.[1−4] Conventional nanomaterial synthesis methods, such as chemical vapor deposition or hydrothermal reaction, usually show a low growth rate. For example, the typical growth rate of ZnO in a hydrothermal process is in the range of a few hundred nanometers per hour.[5−7] The growth rate in vapor depositions could reach a few nanometers per second,[8−10] but it usually requires high temperature which demands a well-controlled environment that is not always compatible with other nanofabrication processes. Moreover, in a conventional hydrothermal reaction, chemical methods are widely studied to control the crystal growth, such as changing the precursor concentration,[11] adjusting pH values,[12] adding capping agents,[13] etc. However, these methods are either less effective, since the intrinsic features of a hydrothermal reaction such as slow rate could not be changed significantly,[14] or easily out of control, such as slightly different pH environment will lead to nanomaterials product with dramatically different morphologies.[15] Therefore, if the deposited nanomaterials can be finely controlled, the potential of laser-induced nanomanufacturing of high productivity and high quality could be a potential method for nanomaterials production in quantity.

The pulsed-laser method provides unique opportunities to control the materials deposition processes and to investigate fundamental mechanisms, due to its promising features in the following aspects: First, the pulsed laser could input thermal energy with high precision, so it provides the driving force of crystal growth in a quantitative manner. Second, since the pulsed laser could input a large dose of energy during a short period of irradiation time, the thermodynamic and kinetic mechanisms of crystal growth may change, and therefore, the novel reaction pathways, such as nucleation and crystal growth, may be observed.[16] Recently, the pulsed-laser method was applied to selectively initiate nucleation in a classical or nonclassical pathway, which provided a deeper understanding of crystallization processes.[17] Third, a pulsed laser is a precise tool with high resolution in special and temporal terms, so it could selectively change the growth condition in a localized region, which will benefit bottom-up integrated nanomanufacturing processes. Lastly, pulsed-laser control of the crystal growth using through a thermodynamic and kinetic manner can realize catalyst-free processes during nucleation and crystal

Received: January 27, 2019
Revised: March 20, 2019
Published: March 25, 2019

DOI: 10.1021/acs.cgd.9b00133
Cryst. Growth Des. 2019, 19, 2912−2918

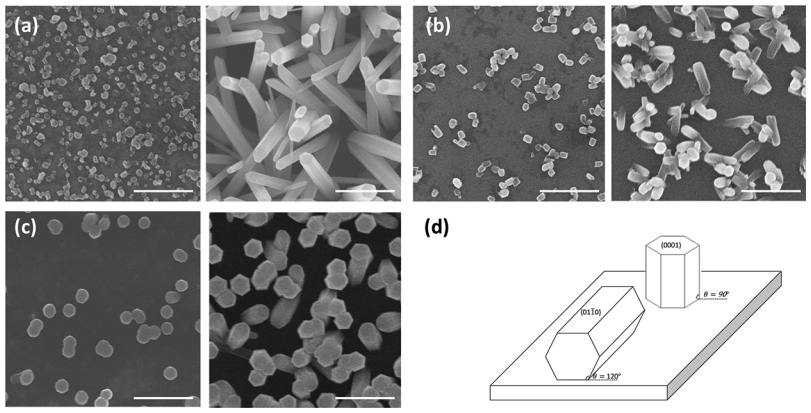

Figure 1. (a–c) Nucleation (left) and corresponding crystal growth (right) under laser irradiation of (a) 0.5 mJ/pulse, (b) 0.25 mJ/pulse, (c) 0.1 mJ/pulse. (d) Schematic diagram of heterogeneous nucleation in (0001) plane with contact angle $\theta = 90°$ and in $\{01\bar{1}0\}$ planes with $\theta = 120°$. All scale bars represent 1 μm in length.

growth. It will contribute to the fundamental understanding of crystallization processes.

In this study, the pulsed-laser method was used for the first time to control the crystal growth in solution-based synthesis by hydrothermal deposition of ZnO, and mechanisms were investigated in thermodynamics and kinetics aspects. ZnO was chosen as the model material because it is a promising 1D nanomaterial in photonics,[18] solar cells,[19] and piezoelectric energy conversion,[20] and it is readily produced by hydrothermal reaction. Morphology, orientation, and dimensions are critical factors for nanowires (NWs)-based devices. For example, the aspect ratio of NWs will affect piezoelectric properties of sensor devices,[21] and the performance of dye-sensitized solar cells is related to the length of ZnO NWs.[22] In this study, the ZnO crystal growth process was investigated by adjusting the laser energy in a stepped variation. By selectively supplying input energy of the pulsed laser to overcome particular energy barriers, crystals with desired orientation morphology could be produced. Morphology related kinetical mechanisms during laser-induced ZnO crystal growth was analyzed by investigating diffusion/reaction-limited factors. On the basis of different behaviors of crystal growth in diffusion- or reaction-limited regions, a set of guidelines were developed to tune the dimensions (diameter, length, and aspect ratio) of NWs crystals.

2. EXPERIMENTAL SECTION

Laser-induced hydrothermal synthesis was carried out at a precursor solution containing 1:1 zinc chloride to hexamethylene tetramine (HMTA) (all chemicals from Sigma-Aldrich) ratio in 20 mM for nucleation process and 5 mM for crystal growth. Additionally, the supersaturation of the precursor solution was set in a low value by adding acid (0.5 mL of dilute nitric acid (HNO_3), pH = 2.3) to the precursor solution to prevent spontaneous reaction at room temperature. The reason to lower the concentration of the precursor solution for crystal growth is to eliminate the additional nucleation that may compete to consume the precursor and therefore inhibit the crystal growth process. Chemical reactions were induced by the thermal decomposition of HMTA, which is only activated by irradiation of a pulsed laser. The reactions referring to the general hydrothermal route are[23]

$$(CH_2)_6N_4 + 6H_2O \rightarrow 6HCHO + 4NH_3$$

$$NH_3 + H_2O \rightleftarrows NH_4^+ + OH^-$$

$$2OH^- + Zn^{2+} \rightleftarrows ZnO + H_2O$$

A substrate of Si(100) with a 300 nm SiO_2 layer in a size of 1 cm × 1 cm was cleaned with DI water and immersed in the 50 mL precursor solution for hydrothermal growth. A ytterbium pulsed fiber laser with a wavelength of 1064 nm, pulse width of 100 ns, and beam size of 200 μm was used to irradiate the substrate to trigger hydrothermal reaction. Pulsed-laser energy varied in a step of 0.05 mJ/pulse from 0.1 to 0.5 mJ/pulse. In the nucleation process, the pulsed laser was set at a low repetition rate of 50 kHz. The substrate was exposed to the laser for 2 s (on time) to induce chemical reaction and covered for 20 s (off time) to prevent the crystal aging induced by heat accumulation. The total exposure time for ZnO nucleation was 2 min. In the NWs growth stage, the pulsed laser was set at a high repetition rate of 200 kHz to provide energy in high frequency. After growth, the substrate was rinsed with DI water and dry. Then scanning electron microscopy (SEM, Hitachi 4800 Field-Emission) was used to image both top-down and cleaved cross-sectional NWs.

3. RESULTS AND DISCUSSION

3.1. Laser Effect on Orientation Control. Orientation of crystals could be controlled by laser-induced chemical deposition in this study, without the need of predeposition of the seed layer or specific crystal structure of substrates. NWs with up-straight orientation were obtained based on heterogeneous nucleation with (0001) planes (*c*-planes) of the ZnO crystal attaching the substrate. Pulsed laser was able to selectively nucleate ZnO in the [0001] orientation by precisely only overcoming the energy barriers required.

By changing the input energy in a step of 0.05 mJ/pulse, the energy barriers of different nucleation processes could be determined. It was observed in our experiment that a large energy input of 0.5 mJ/pulse will lead to homogeneous nucleation, and the crystal grown from the homogeneous nuclei will be randomly oriented, as shown in Figure 1a. When the laser power is decreased to 0.25 mJ/pulse, nucleation will transfer from a homogeneous to a heterogeneous way. Only a single layer of crystals formed on the substrate surface but without orientation preference shown, so the crystals growth afterward was also in a single layer but randomly oriented (Figure 1b). If the laser power decreased to the level just above the threshold of nucleation, below which nucleation will not be triggered, as 0.1 mJ/pulse determined in our experiment, most nuclei will have the *c*-axis perpendicular to the substrates, and the corresponding NWs will have up-straight orientation (Figure 1c).

DOI: 10.1021/acs.cgd.9b00133
Cryst. Growth Des. 2019, 19, 2912–2918

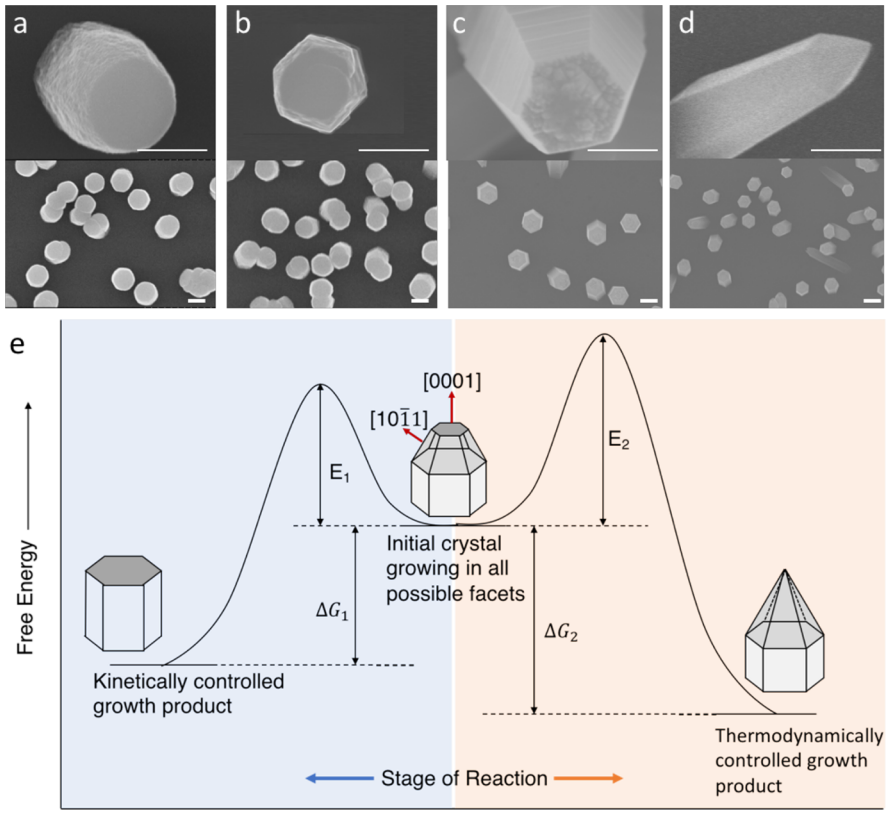

Figure 2. SEM pictures of ZnO crystals grown under laser power density of (a) 9.55 kW/cm^2, (b) 15.92 kW/cm^2, (c) 22.29 kW/cm^2, (d) 28.66 kW/cm^2 in 200 kHz for 5 min. (e) Schematic illustration of crystal growth in kinetically controlled (left direction) and thermodynamically controlled (right direction) processes. All scale bars represent 500 nm in length.

According to the classical nucleation theory, the energy barriers ΔG_{hom} of homogeneous nucleation could be described by

$$\Delta G_{hom} = \frac{16\pi\gamma^3}{3(\Delta G_v)^2}$$

where γ is the interfacial tension between the nuclei and solution, ΔG_v is the specific free energy change associated with the liquid−solid phase change per unit volume. The energy barriers for heterogeneous nucleation are $\Delta G_{het} = \Delta G_{hom} f(\theta)$, which is smaller than homogeneous nucleation due to the structure factor $f(\theta)$[24]

$$f(\theta) = (2 - 3\cos\theta + \cos^3\theta)/4$$

where θ is the contact angle between nuclei and substrate, as shown in Figure 1d. Specifically, if ZnO heterogeneously nucleated with the (0001) facet contacting with the substrate, the structure factor would be $f(\theta) = (90°) = 0.5$. If it is nucleated with the (01$\bar{1}$0) surface, the contact angle would be 120° and the energy barrier would be 0.843 ΔG_{hom}. So the energy barriers under different conditions will have the relationship of $\Delta G_{hom} > \Delta G_{het\_random} > \Delta G_{het\_(0001)}$. The experimental results are corresponding to the classical nucleation theory. By adjusting the laser energy input just above the minimum energy barriers $\Delta G_{het\_(0001)}$, which corresponds to the heterogeneous nucleation with the *c*-plane attaching to the substrate, NWs with an orientation of [0001] perpendicular to the substrate could be obtained.

Although changing precursor solution could also control crystallization by adjusting the nucleation energy barriers,[25] i.e., energy barriers are lower in solution with high concentration and vice versa, fluctuations in bulk solution make it hard to confine energy in a narrow range. Therefore, homogeneous, heterogeneous nucleation, and crystal growth process could hardly be isolated and studied independently in conventional hydrothermal reactions. A pulsed laser, as a precise tool to thermally trigger the crystallization process, could input a large dose of energy in a short period of nanoseconds range of time. In this unique condition, the crystallization process could happen even when supersaturation and kinetics for phase transformation were set at sufficiently low values.[17,26] Therefore, the effect of input energy dominates and the energy fluctuations caused by nonuniformity of precursor solution could be ignored.

3.2. Laser Effect on Morphology Control. It is generally believed that ZnO prefers to grow along the *c*-axis (the [0001] direction), in which the total surface energy could remain minimum during crystal growth.[27] In this study, crystal morphology could be controlled in a more precise manner. Not only (0001) but also other surfaces with higher Miller indices were selectively obtained by the pulsed-laser method.

Our experimental results showed that a specific crystal structure occurs only if a certain input energy level was reached by the laser. By selectively setting the laser power, the crystal will grow with a desired morphology. When the input power was below 9.55 kW/cm^2, all crystal surfaces were activated at a very low rate, and the crystal would undergo a homogeneous growth and result in a spherical structure (Figure 2a). When the power was increased from 9.55 to 15.92 kW/cm^2, the energy barriers for growth of prismatic planes (*m*-planes) were overcome, resulting in a transformation from a cylinder to a

DOI: 10.1021/acs.cgd.9b00133
Cryst. Growth Des. 2019, 19, 2912−2918

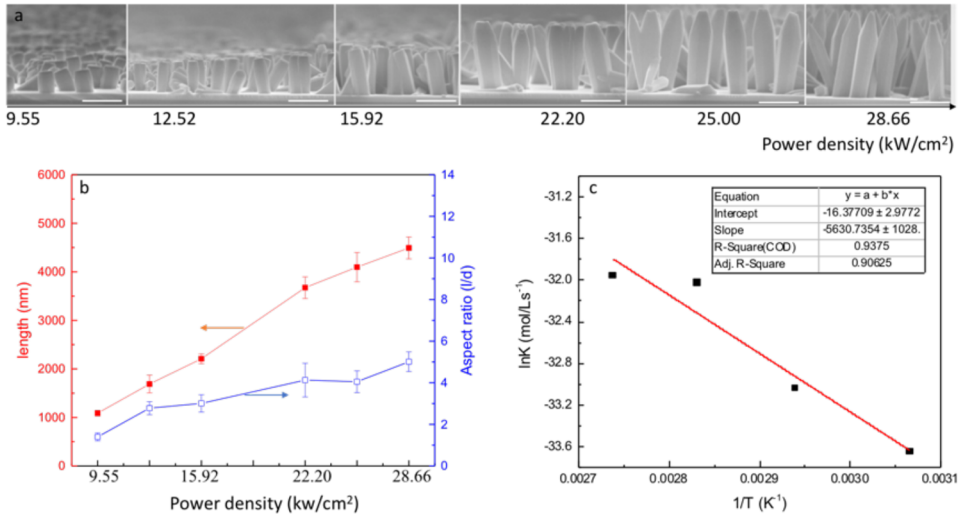

Figure 3. (a) SEM cross-sectional pictures of NWs grown under power density from 9.55 to 28.66 kW/cm^2 (left to right) in 200 kHz for 5 min; all scale bars represent 2 μm. (b) Corresponding length and aspect ratio of NWs. (c) Arrhenius plot for the crystal growth process.

hexagonal shape (Figure 2b). It indicated that the energy barriers of growth along $\langle 10\bar{1}1\rangle$, $\langle 10\bar{1}0\rangle$ are overcome but not [0001] (*c*-axis). Therefore, the growth rate of $\{10\bar{1}1\}$ planes is higher than (0001) and results in a flat surface on the crystal tip. When the pulsed-laser power increased to 22.29 kW/cm^2, the crystal would grow along the preferred orientation of the *c*-axis. It indicated that energy barriers of growth of (0001) planes were overcome, so that the growth rate of (0001) planes increased dramatically and led the crystal to grow longer. As shown in Figure 2c,d, when the pulsed-laser power increased above 22.29 kW/cm^2, the tip did not grow smooth but instead was bounded by hillocks which were composed of faces of higher Miller indices and tips of crystals tend to approach $\{10\bar{1}1\}$. Faces of hillocks have lower specific surface free energy than (0001), so that these higher Miller indices faces predominate. When the pulsed-laser power was above 28.66 kW/cm^2, the (0001) surface had the highest growth rate that led to a pyramid-like crystal structure. It is worth noting that it is the peak power rather than the accumulated energy that overcomes the energy barriers. Evidence of this statement could be found that the certain morphology grown under a specific high power density that will not occur in the condition of irradiation by lower power accumulated for a longer time, even though the total energy input is the same. For example, the total irradiation energy by a laser power density of 15.92 kW/cm^2 for 1.4 min is the same with 22.29 kW/cm^2 irradiation for 1 min. However, the hillocks structure which indicated the activation of burst growth along the [0001] direction was not found in a laser condition of 15.92 kW/cm^2, even when irradiated for 40 min.

Two paths could be identified by laser-induced crystal growth. In the kinetically controlled path, as shown in the reaction in the left direction in Figure 2e, the crystal is controlled by energy barriers of growth along specific surfaces. The crystal growth is generally regarded as a process of 2D nucleation of an island on the terraces, followed by lateral motion of steps.[28] The 2D nucleation of an island is similar to initial heterogeneous nucleation, in which the free energy barrier, *E*, relates to surface energy of the specific plane, $E \propto \frac{\gamma^3}{\Delta G_v^2}$. γ has different values along different planes. The surface energy of prismatic planes $\{10\bar{1}0\}$ is 1.15 J/m^2, and 1.37 J/m^2 for $\{10\bar{1}1\}$ planes, and for the basal plane surface (0001), it is 2.0 J/m^2.[29,30] Therefore, the energy barriers for crystal growth of planes are in the order of $\{0001\} > \{10\bar{1}1\} > \{10\bar{1}0\}$. Our experimental results showed that the occurrence of crystal planes with increasing energy inputs followed the sequence of $\{10\bar{1}0\}$, $\{10\bar{1}1\}$, {0001}, which was in the same order of surface energy values cited above. When the input energy is not large enough to overcome the energy barriers of 2D nucleation on all crystal planes, the certain planes with low energy barriers will be formed first, and planes with higher energy barriers not overcome will grow at a low rate. For example, when the input power is below 22.29 kW/cm^2, large enough to induce growth along $\langle 10\bar{1}1\rangle$ but not enough to overcome the energy barriers of 2D nucleation on the (0001) surface, the crystal growth process is limited by kinetic factors of (0001), so that the growth rate of $\{10\bar{1}1\}$ is larger than that of (0001), and results in a hexagonal morphology with a flat surface on the tip (as shown in Figure 2b and illustrated in the left direction in Figure 2e). When the input energy increases and is able to overcome the energy barriers of growth along all planes, the surface reaction is not the limited factor and the growth of (0001) is not inhibited anymore. In this circumstance, crystal growth will undergo a thermodynamically controlled pathway, as illustrated in the reaction in the right direction (Figure 2e), where the product with the largest Gibbs energy ΔG will be preferred to form because it is the most thermodynamically stable state. The Gibbs energy ΔG reaches maximum when the total surface energy $\sum \sigma A$ of the crystal remains minimum as the crystal grows. It could be measured by the increase of surface energy per volume $d\sum \sigma A/dv$. As calculated, $d\sum \sigma A/dv$ is 12.69J/m in a hexagonal structure and 10.63 J/m in a pyramid-like structure on the crystal tip. It indicated that the pyramid-like structure is more stable than the hexagonal structure in the thermodynamically controlled reaction. Therefore, when the input energy is high enough (above 28.66 kW/cm^2), the ZnO crystal will have the morphology of the pyramid-like structure on the tip (Figure 2d).

3.3. Laser Effect on Growth Rate. NWs usually grow at a low rate and were thought to be limited by the mass-transfer process in the conventional hydrothermal reaction.[31] In this study, the same slow growth habit of crystal particles was also

DOI: 10.1021/acs.cgd.9b00133
Cryst. Growth Des. 2019, 19, 2912−2918

observed when the laser power density is below 9.55 kW/cm^2, as shown in Supporting Information Figure S1. However, a rapid growth rate of NWs could be obtained when increasing the laser energy input, and different kinetic mechanisms were observed. By tracking dimensions of NWs under different conditions of laser irradiation, the kinetics mechanism in the laser-induced hydrothermal reaction was revealed in a comprehensive way.

ZnO crystals in this work begin to grow at a high rate, and growth rate is sensitive to the temperature change induced by laser input energy. Generally, *c*-planes have higher growth rate than *m*-planes, and higher power density results in higher growth rate. The anisotropic growth and the temperature-related growth rate show the typical characteristics of reaction-limited growth. SEM pictures in Figure 3a show the cross sections of ZnO crystals grown under different laser power densities for 5 min. ZnO crystals grow into nanorods with different lengths. The anisotropic morphology could be described by aspect ratio and length/diameter (l/d), as shown in Figure 3b. When the laser power density is increased from 9.55 to 28.66 kW/cm^2, the length of ZnO crystals increases from 1.09 to 4.49 μm, and the aspect ratio increases from 1.40 to 5.01.

It is worth noting that the laser-induced method has a much higher growth rate than conventional hydrothermal[5−7] and other methods reported, such as electrochemically assisted[33] and microwave-assisted growth.[34,37] Different growth rates are compared in Table 1. This remarkable fast growth rate may be attributed to (1) enhanced mass transport, which was reported by another localized synthesis study,[38] (2) suppression of precursor depletion by additional nucleation, and (3) a rapid heating process which could reduce the time needed for reaching the crystallization temperature.[37] According to simulation results (Supporting Information Figure S2), the temperature profile of the laser-assisted hydrothermal method could reach equilibrium within a short period of time (<0.01 s).

Table 1. Comparison of Growth Rate of ZnO NWs under Different Hydrothermal Reactions

reaction method	rate (μm/min)	relative rate	reference
conventional hydrothermal	<0.02	<1	5−7
sonochemical	0.008	1	32
continuous flow reactor	0.033	4.125	13
electrochemically assisted	0.125	15.625	33
microwave-assisted	0.300	37.5	34
CW laser-assisted	0.333	41.625	35
pulsed-laser-induced reaction	0.6.−6	75−750	36 and this work

In the reaction-limited region, increasing the intensity of the laser power is an effective way to accelerate the growth rate. The relationship between reaction rate constant and temperature is then given by the Arrhenius equation

$$k = Ae^{-E_a/RT}$$

where E_a is the activation energy, which is equal to the energy barriers in the crystal growth process, R is the universal gas constant, and A represents the pre-exponential factor, which is a constant for the reaction. The activation energy E_a could be obtained from the slope of the Arrhenius diagram plotted with the natural logarithm of the rate constants versus the inverse temperature, as shown in Figure 3c. The obtained activation energy E_a is about 46.8 kJ/mol, which is in the range of dehydration barrier values reported (40−80 kJ/mol), but lower than those reported in a conventional hydrothermal reaction of 65 kJ mol^{-1}.[39] It indicated that a pulsed laser may also induce a lower activation energy, and therefore lead to a high growth rate under the same condition with the conventional hydrothermal reaction.

3.4. Laser Effect on Kinetic Mechanisms. When continuing to supply laser power, the crystals with a hexagonal structure and pyramid-like structure show very different growth behavior, as shown in Figure 4a,b. The length and aspect ratio change over time as shown in Supporting Information Figure S3. Correspondingly, the growth rate of the *c*-plane of the hexagonal crystal reached 250 nm/min in the first 2 min, but slowed down after 20 min. The length of crystals did not change much after 20 min, and *c*- and *m*-planes almost have the same growth rate (Figure 4c).

The diffusion/reaction-limited analysis[31] is applied to study the kinetic mechanisms of crystal growth by considering the relationship of consumption of precursor ions at the crystal surface, and the diffusive transport in the bulk solution. The ratio of surface reaction rate to reactant diffusion to the crystal growth front could be measured by the Thiele modulus[40]

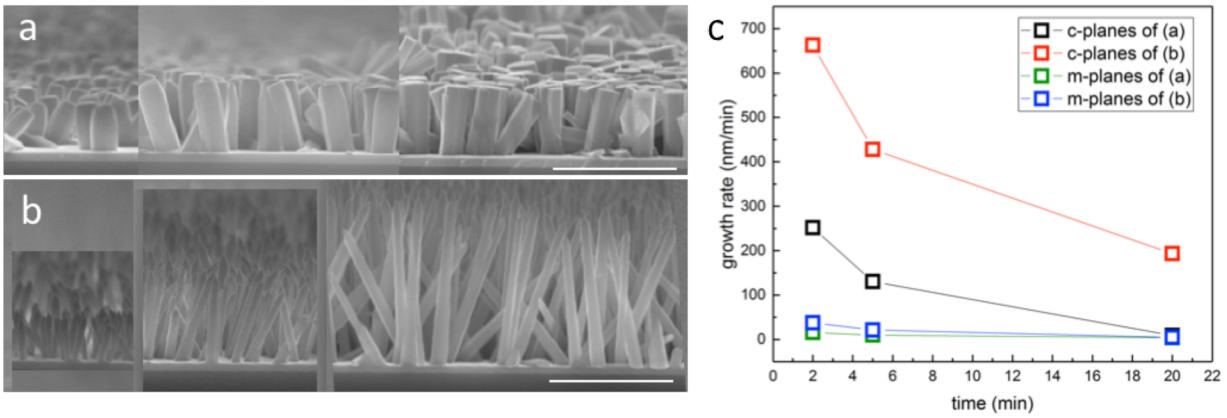

Figure 4. SEM pictures of cross sections of crystals grown under (a) 15.92 kW/cm^2 and (b) 28.66 kW/cm^2 for 2, 5, and 20 min, respectively. (c) Corresponding growth rate of *c*-plane and *m*-planes of ZnO crystals shown in (a) and (b). All scale bars represent 5 μm.

DOI: 10.1021/acs.cgd.9b00133
Cryst. Growth Des. 2019, 19, 2912−2918

$$\phi = \frac{kS\delta}{D}$$

where D is the Zn^{2+} aqueous tracer diffusion coefficient, δ is the stagnant layer thickness, and S is the modified factor representing the c-plane area ratio. As the hexagonal crystal grows along both c-plane and m-planes, the c-plane area ratio, S, keeps increasing during the growth of hexagonal crystals. Therefore, there will be a transfer from the reaction-limited region, where $\phi < 1$, to the diffusion-limited region, where $\phi > 1$. The growth rate along the c-axis could be described by[31]

$$\frac{dh}{dt} = \frac{kC_\infty}{\rho(1 + \varnothing)}$$

where h represents the height of NWs, C_∞ is the bulk solution concentration of Zn^{2+}, and ρ is the ZnO molar density. The hexagonal crystals grew under reaction limitation first (within 5 min), when the crystals grew faster along the c-axis and led to a dramatic increase in aspect ratio. After 20 min, the crystals grew homogeneously at a low rate, which indicated that growth was limited by mass transfer.

Crystals with a pyramid-like structure on the tip show different growth behavior. They grew faster than hexagonal crystals, especially in the c-axis and resulted in a morphology with higher aspect ratio. Specifically, the growth rate of the c-plane of the pyramid-like crystal could reach 660 nm/min in the first 2 min, which is almost 3 times than hexagonal crystals and even 30 times than the conventional hydrothermal reaction. Although the growth rate of c-planes also decreased with time, it always kept higher than the growth rate of m-planes. The anisotropic growth indicated that the growth of pyramid-like crystals was always reaction-limited. The rapid growth may be due to two main reasons: First, the activated c-planes are favored by 2D nucleation, and the large amount of 2D nucleation cited acts as high density kinks which kinetically facilitate crystal growth along the c-direction. Second, as the crystal tip shows a pyramid-like structure, the c-plane area ratio, S, always remains in a low value. Therefore, the diffusion of precursor ions is always enough to the tip and prevents the crystal growth to be inhibited by mass transfer. In the reaction-limited region, where $\phi \ll 1$, growth rate is independent of the NWs diffusion environment. The relationship of growth rate with reaction kinetic factor could then be described by

$$\frac{dh}{dt} \approx \frac{kC_\infty}{\rho}$$

The surface reaction rate constant k of c-planes of the pyramid-like crystal was determined to be 4.59×10^{-5} ms^{-1}, which is 14.40 times than the conventional hydrothermal reaction rate.[39] The different growth behavior in two regions provided guidance for dimension and aspect ratio control. As reaction-limited growth results in an anisotropic morphology, increasing the power density of the laser could differentiate the growth rate of different crystal surfaces and lead to long NWs with higher aspect ratio. Diffusion controlled growth typically results in homogeneous growth, by which crystals grow uniformly with a constant aspect ratio.

4. CONCLUSIONS

Laser-induced chemical deposition is a promising bottom-up method to fabricate nanomaterials. It could effectively boost growth rate and tune the orientation, morphology, and dimensions of NWs. NWs with up-straight orientation could be obtained by setting the laser energy input to just overcome the lowest nucleation energy barrier, which is corresponding to the heterogeneous nucleation with c-planes attaching to substrates. The mechanism of laser-induced morphology control was studied kinetically and thermodynamically. Different morphologies of crystals could be obtained by adjusting the laser energy to selectively overcome the energy barriers of different surfaces. After kinetic barriers are overcome, crystals will stay in a thermodynamically stable state, which minimizes the total surface free energy. By adjusting the laser power density according to different mechanisms in reaction- and diffusion-limited regions, NWs with desired dimensions and morphology could be obtained. Laser-induced chemical deposition is also a precise tool to investigate the mechanisms of nucleation and crystal growth from thermodynamic and kinetic points of view and provides guidelines for fabricating nanomaterials with desired morphology for a wide variety of specific device purposes.

■ ASSOCIATED CONTENT

Supporting Information

The Supporting Information is available free of charge on the ACS Publications website at DOI: 10.1021/acs.cgd.9b00133.

S1: Diffusion-limited nanoparticles growth. S2: Simulation of the temperature profile. S3: Length and aspect ratio change over time (PDF)

■ AUTHOR INFORMATION

Corresponding Author

*E-mail: liuch@purdue.edu.

ORCID

Siyu Liu: 0000-0002-8059-283X

Notes

The authors declare no competing financial interest.
Some ideas covered in this paper are patent pending.

■ ACKNOWLEDGMENTS

The project was partially supported by NSF (CMMI) Grant 1663214.

■ REFERENCES

(1) Liu, Z.; Liu, C. R. Laser-Induced Solution Synthesis and Deposition: A Generic Method to Make Metal Chalcogenide Nanotubes at High Rate with High Consistency. *Proc. Inst. Mech. Eng., Part N* **2014**, *228*, 66−72.

(2) Liu, Z.; Liu, C. R. Methods of Forming Nano-Scale and Micro-Scale Structured Materials and Materials Formed Thereby. U.S. Patent Application No. 14/864235, 2015.

(3) Liu, Z.; Cao, Z.; Deng, B.; Wang, Y.; Shao, J.; Kumar, P.; Liu, C. R.; Wei, B.; Cheng, G. J. Ultrafast and Scalable Laser Liquid Synthesis of Tin Oxide Nanotubes and Its Application in Lithium Ion Batteries. *Nanoscale* **2014**, *6*, 5853−5858.

(4) Liu, Z.; Richard Liu, C. Laser Induced Chemical Deposition of Ferrihydrite Nanotubes: Exploring Growth Rate and Crystal Structure. *J. Micro Nano-Manuf.* **2014**, *2*, 011001.

(5) Vayssieres, L. Growth of Arrayed Nanorods and Nanowires of ZnO from Aqueous Solutions. *Adv. Mater.* **2003**, *15*, 464−466.

(6) Greene, L. E.; Law, M.; Goldberger, J.; Kim, F.; Johnson, J. C.; Zhang, Y.; Saykally, R. J.; Yang, P. Low-Temperature Wafer-Scale Production of ZnO Nanowire Arrays. *Angew. Chem., Int. Ed.* **2003**, *42*, 3031−3034.

DOI: 10.1021/acs.cgd.9b00133
Cryst. Growth Des. 2019, 19, 2912−2918

(7) Tian, Z. R.; Voigt, J. A.; Liu, J.; Mckenzie, B.; Mcdermott, M. J.; Rodriguez, M. A.; Konishi, H.; Xu, H. Complex and Oriented ZnO Nanostructures. *Nat. Mater.* **2003**, *2*, 821−826.
(8) Kar, S.; Pal, B. N.; Chaudhuri, S.; Chakravorty, D. One-Dimensional ZnO Nanostructure Arrays: Synthesis and Characterization. *J. Phys. Chem. B* **2006**, *110*, 4605−4611.
(9) Wang, X.; Summers, C. J.; Wang, Z. L. Large-Scale Hexagonal-Patterned Growth of Aligned ZnO Nanorods for Nano-Optoelectronics and Nanosensor Arrays. *Nano Lett.* **2004**, *4*, 423−426.
(10) Podrezova, L. V.; Porro, S.; Cauda, V.; Fontana, M.; Cicero, G. Comparison between ZnO Nanowires Grown by Chemical Vapor Deposition and Hydrothermal Synthesis. *Appl. Phys. A: Mater. Sci. Process.* **2013**, *113*, 623−632.
(11) Cao, H. L.; Qian, X. F.; Gong, Q.; Du, W. M.; Ma, X. D.; Zhu, Z. K. Shape- and Size-Controlled Synthesis of Nanometre ZnO from a Simple Solution Route at Room Temperature. *Nanotechnology* **2006**, *17*, 3632−3636.
(12) Yamabi, S.; Imai, H. Growth Conditions for Wurtzite Zinc Oxide Films in Aqueous Solutions. *J. Mater. Chem.* **2002**, *12*, 3773−3778.
(13) Joo, J.; Chow, B. Y.; Prakash, M.; Boyden, E. S.; Jacobson, J. M. Face-Selective Electrostatic Control of Hydrothermal Zinc Oxide Nanowire Synthesis. *Nat. Mater.* **2011**, *10*, 596−601.
(14) Tak, Y.; Yong, K. Controlled Growth of Well-Aligned ZnO Nanorod Array Using a Novel Solution Method. *J. Phys. Chem. B* **2005**, *109*, 19263−19269.
(15) Govender, K.; Boyle, D. S.; Kenway, P. B.; O'Brien, P. Understanding the Factors That Govern the Deposition and Morphology of Thin Films of ZnO from Aqueous Solution. *J. Mater. Chem.* **2004**, *14*, 2575.
(16) Bäuerle, D. *Laser Processing and Chemistry*, 4th ed.; Springer: Berlin, 2011.
(17) Liu, Z.; Liu, C. R. Nucleation of Hematite Nanocrystals Revealed by a Single Nanoseconds Laser Pulse Method. *Nanoscale* **2018**, *10*, 14400−14405.
(18) Huang, M. H.; Mao, S.; Feick, H.; Yan, H.; Wu, Y.; Kind, H.; Weber, E.; Russo, R.; Yang, P. Room-Temperature Ultraviolet Nanowire Nanolasers. *Science* **2001**, *292*, 1897−1900.
(19) Law, M.; Greene, L. E.; Johnson, J. C.; Saykally, R.; Yang, P. Nanowire Dye-Sensitized Solar Cells. *Nat. Mater.* **2005**, *4*, 455−459.
(20) Song, J.; Zhou, J.; Wang, Z. L. Piezoelectric and Semiconducting Coupled Power Generating Process of a Single ZnO Belt/Wire. A Technology for Harvesting Electricity from the Environment. *Nano Lett.* **2006**, *6*, 1656−1662.
(21) Wang, Z. L.; Song, J. Piezoelectric Nanogenerators Based on Zinc Oxide Nanowire Arrays. *Science* **2006**, *312*, 242−246.
(22) Ko, S. H.; Lee, D.; Kang, H. W.; Nam, K. H.; Yeo, J. Y.; Hong, S. J.; Grigoropoulos, C. P.; Sung, H. J. Nanoforest of Hydrothermally Grown Hierarchical ZnO Nanowires for a High Efficiency Dye-Sensitized Solar Cell. *Nano Lett.* **2011**, *11*, 666−671.
(23) Schmidt-mende, L.; Macmanus-driscoll, J. L. Defects, and Devices ZnO Has Received Much Attention over the Past Few Years Because. *Mater. Today* **2007**, *10*, 40−48.
(24) Fujihara, S.; Sasaki, C.; Kimura, T. Crystallization Behavior and Origin of C-Axis Orientation in Sol-Gel-Derived ZnO:Li Thin Films on Glass Substrates. *Appl. Surf. Sci.* **2001**, *180*, 341−350.
(25) Tao, A. R.; Habas, S.; Yang, P. Shape Control of Colloidal Metal Nanocrystals. *Small* **2008**, *4*, 310−325.
(26) Liu, Z.; Richard Liu, C. Laser induced chemical solution deposition of nanomaterials: a novel process demonstrated by manufacturing SnO2 nanotubes. *Manuf. Lett.* **2013**, *1*, 42−45.
(27) Wang, Z. L. Zinc Oxide Nanostructures: Growth, Properties and Applications. *J. Phys.: Condens. Matter* **2004**, *16*, R829−R858.
(28) De Yoreo, J. J. Principles of Crystal Nucleation and Growth. *Rev. Mineral. Geochem.* **2003**, *54*, 57−93.
(29) Yoon, H.; Yi, G.-C. Position-Controlled Selective Growth of ZnO Nanostructures and Their Heterostructures. In *Semiconductors and Semimetals*, 1st ed.; Elsevier Inc.: Amsterdam, 2015; Vol. 93.
(30) Na, S.-H.; Park, C.-H. First-Principles Study of the Surface of Wurtzite ZnO and ZnS-Implications for Nanostructure Formation. *J. Korean Phys. Soc.* **2009**, *54*, 867−872.
(31) Boercker, J. E.; Schmidt, J. B.; Aydil, E. S. Transport Limited Growth of Zinc Oxide Nanowires. *Cryst. Growth Des.* **2009**, *9*, 2783−2789.
(32) Jung, S. H.; Oh, E.; Lee, K. H.; Park, W.; Jeong, S. H. A Sonochemical Method for Fabricating Aligned ZnO Nanorods. *Adv. Mater.* **2007**, *19*, 749−753.
(33) Cui, J.; Gibson, U. J. Enhanced Nucleation, Growth Rate, and Dopant Incorporation in ZnO Nanowires. *J. Phys. Chem. B* **2005**, *109*, 22074−22077.
(34) Mahpeykar, S. M.; Koohsorkhi, J.; Ghafoori-Fard, H. Ultra-Fast Microwave-Assisted Hydrothermal Synthesis of Long Vertically Aligned ZnO Nanowires for Dye-Sensitized Solar Cell Application. *Nanotechnology* **2012**, *23*, 165602.
(35) Yeo, J.; Hong, S.; Wanit, M.; Kang, H. W.; Lee, D.; Grigoropoulos, C. P.; Sung, H. J.; Ko, S. H. Rapid, One-Step, Digital Selective Growth of ZnO Nanowires on 3D Structures Using Laser Induced Hydrothermal Growth. *Adv. Funct. Mater.* **2013**, *23*, 3316−3323.
(36) Liu, Z.; Liu, C. R. Laser-Induced Solution Synthesis and Deposition : A Generic Method To Make Metal Chalcogenide Nanotubes at High Rate with High Consistency. *Proc. Inst. Mech. Eng., Part N* **2014**, *228*, 66−72.
(37) Unalan, H. E.; Hiralal, P.; Rupesinghe, N.; Dalal, S.; Milne, W. I.; Amaratunga, G. A. J. Rapid Synthesis of Aligned Zinc Oxide Nanowires. *Nanotechnology* **2008**, *19*, 255608.
(38) Yang, D.; Kim, D.; Ko, S. H.; Pisano, A. P.; Li, Z.; Park, I. Focused Energy Field Method for the Localized Synthesis and Direct Integration of 1D Nanomaterials on Microelectronic Devices. *Adv. Mater.* **2015**, *27*, 1207−1215.
(39) Cheng, J. J.; Nicaise, S. M.; Berggren, K. K.; Gradečak, S. Dimensional Tailoring of Hydrothermally Grown Zinc Oxide Nanowire Arrays. *Nano Lett.* **2016**, *16*, 753−759.
(40) Thiele, E. W. Relation between Catalytic Activity and Size of Particle. *Ind. Eng. Chem.* **1939**, *31*, 916−920.

DOI: 10.1021/acs.cgd.9b00133
Cryst. Growth Des. 2019, 19, 2912−2918